BIOLOGICAL CRYSTALLOGRAPHY

ISSN 1399-0047

# Structural and functional evidence for membrane docking and disruption sites on phospholipase $A_2$-like proteins revealed by complexation with the inhibitor suramin

Guilherme H. M. Salvador,[a] Thiago R. Dreyer,[a] Walter L. G. Cavalcante,[a] Fábio F. Matioli,[a] Juliana I. dos Santos,[a] Adrian Velazquez-Campoy,[b,c] Márcia Gallacci[d] and Marcos R. M. Fontes[a]*

[a]Department of Physics and Biophysics, Institute of Biosciences, UNESP – Universidade Estadual Paulista, Botucatu-SP, Brazil, [b]Institute of Biocomputation and Physics of Complex Systems (BIFI), Joint Unit IQFR–CSIC–BIFI and Department of Biochemistry and Molecular and Cell Biology, University of Zaragoza, Zaragoza, Spain, [c]Fundacion ARAID, Government of Aragon, Zaragoza, Spain, and [d]Department of Pharmacology, Institute of Biosciences, UNESP – Universidade Estadual Paulista, Botucatu-SP, Brazil. *Correspondence e-mail: fontes@ibb.unesp.br

Received 6 May 2015
Accepted 31 July 2015

Edited by J. L. Martin, University of Queensland, Australia

**Keywords:** phospholipase $A_2$-like proteins; myotoxic mechanism; snakebite envenomation; suramin.

**PDB reference**: myotoxin II from *Bothrops moojeni* complexed with suramin, 4yv5

**Supporting information**: this article has supporting information at journals.iucr.org/d

Local myonecrosis resulting from snakebite envenomation is not efficiently neutralized by regular antivenom administration. This limitation is considered to be a significant health problem by the World Health Organization. Phospholipase $A_2$-like ($PLA_2$-like) proteins are among the most important proteins related to the muscle damage resulting from several snake venoms. However, despite their conserved tertiary structure compared with $PLA_2$s, their biological mechanism remains incompletely understood. Different oligomeric conformations and binding sites have been identified or proposed, leading to contradictory data in the literature. In the last few years, a comprehensive hypothesis has been proposed based on fatty-acid binding, allosteric changes and the presence of two different interaction sites. In the present study, a combination of techniques were used to fully understand the structural–functional characteristics of the interaction between suramin and MjTX-II (a $PLA_2$-like toxin). *In vitro* neuromuscular studies were performed to characterize the biological effects of the protein–ligand interaction and demonstrated that suramin neutralizes the myotoxic activity of MjTX-II. The high-resolution structure of the complex identified the toxin–ligand interaction sites. Calorimetric assays showed two different binding events between the protein and the inhibitor. It is demonstrated for the first time that the inhibitor binds to the surface of the toxin, obstructing the sites involved in membrane docking and disruption according to the proposed myotoxic mechanism. Furthermore, higher-order oligomeric formation by interaction with interfacial suramins was observed, which may also aid the inhibitory process. These results further substantiate the current myotoxic mechanism and shed light on the search for efficient inhibitors of the local myonecrosis phenomenon.

## 1. Introduction

Myonecrosis is an important local effect of envenomations caused by snakebite accidents, which is not efficiently neutralized by regular antivenom administration and may evolve to permanent tissue loss, amputation and victim disability (Lomonte *et al.*, 2003; Otero *et al.*, 2002). This toxic manifestation is particularly serious in accidents involving viperid snakes from the *Bothrops* genus, which are frequent in Latin America (de Oliveira, 2009; Williams *et al.*, 2010). Myonecrosis results from the synergic action of different venom components, including haemorrhagic metalloproteinases that induce ischaemia and the myotoxic phospholipases $A_2$, which promote direct cytotoxicity towards skeletal muscle

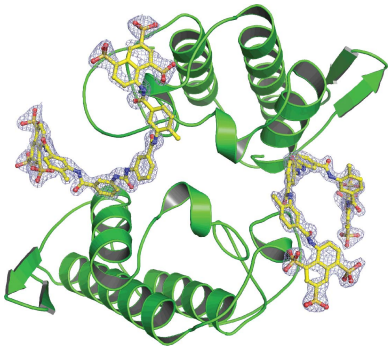

© 2015 International Union of Crystallography

cells (Gutiérrez *et al.*, 2009). Phospholipases $A_2$ ($PLA_2$s; EC 3.1.1.4) comprise a large family of proteins that exhibit similar tertiary structures and are widely found in snake venoms (Dennis *et al.*, 2011; Gutiérrez & Lomonte, 2013). $PLA_2$-like proteins (or $PLA_2$ homologues) comprise an important subclass of these proteins that are often present in viperid venoms, which are catalytically inactive because of a lack of $Ca^{2+}$ coordination related to natural mutations of the Asp49 and Tyr28 residues (Fernandes *et al.*, 2010; Holland *et al.*, 1990). $PLA_2$-like proteins, particularly Lys49-$PLA_2$s (with an Asp49Lys mutation), are intriguing proteins. They are small proteins with conserved tertiary structure whose functions are usually associated with oligomeric conformation changes and different functional sites (Fernandes *et al.*, 2014). Crystallographic, biophysical, biochemical and functional studies aiming to understand the structural basis for myotoxic activity have been performed, resulting in some consistent results and interesting hypotheses (for a recent review, see Fernandes *et al.*, 2014). The most feasible and broad mechanism involves the toxin in a particular dimeric conformation (known as an 'alternative dimer' or a 'compact dimer') that undergoes an oligomeric change after fatty-acid binding, resulting in membrane docking by a cationic site (MDoS) and ultimately in membrane disruption by a hydrophobic site (MDiS; Fernandes *et al.*, 2013).

Structural experiments have been performed with complexes formed of $PLA_2$-like proteins and molecules that are potentially capable of neutralizing their biological activities (de Oliveira *et al.*, 2003; Lomonte *et al.*, 2009; Marcussi *et al.*, 2007; Murakami *et al.*, 2005, 2007; Ticli *et al.*, 2005). Some of these molecules may also serve as models for the design of drugs with anti-ophidian properties and therefore may also be applicable as supplements to conventional serum therapy (Marcussi *et al.*, 2007). Suramin [8,8′-{carbonylbis[imino-3,1-phenylenecarbonylimino(4-methyl-3,1-phenylene)carbonylimino]}di(1,3,5-naphtalenetrisulfonic acid) hexasodium salt] is one such compound because of its neutralizing properties against the myotoxicity of Lys49-$PLA_2$s (Arruda *et al.*, 2002; de Oliveira *et al.*, 2003). This synthetic molecule is a highly charged polysulfonated compound that has been used clinically to treat African trypanosomiasis and onchocerciasis (Burch & Ashburn, 1951; Cherry, 1960; Murakami *et al.*, 2005; Schneider, 1963; Williamson & Desowitz, 1956). When investigated with snake venoms, suramin was shown to inhibit the neuromuscular blockade induced by pre-synaptic neurotoxins such as crotoxin and $\beta$-bungarotoxin (Fathi *et al.*, 2011; Lin-Shiau & Lin, 1999) and prevent the muscle necrosis promoted by BthTX-I, a Lys49-$PLA_2$ from *B. jararacussu* venom (de Oliveira *et al.*, 2003; Arruda *et al.*, 2002).

We have recently performed structural and functional studies of MjTX-II, a myotoxic Lys49-$PLA_2$ from *B. moojeni* (Salvador, Cavalcante *et al.*, 2013). These experiments revealed that this toxin presents structural peculiarities compared with other Lys49-$PLA_2$s that influence ligand binding at the hydrophobic channel of the toxin. Furthermore, we also demonstrated using myographic studies that MjTX-II produces an irreversible and time-dependent blockage of directly and indirectly evoked twitches, similar to other Lys49-$PLA_2$s (Cavalcante *et al.*, 2005, 2007; de Oliveira *et al.*, 2003; Heluany *et al.*, 1992; dos Santos, Cardoso *et al.*, 2011; Gallacci *et al.*, 2006; Oshima-Franco *et al.*, 2004; Randazzo-Moura *et al.*, 2008; Ponce-Soto *et al.*, 2009; Rodrigues *et al.*, 2004; Stábeli *et al.*, 2006; Soares *et al.*, 2001; Salvador, Fernandes *et al.*, 2013).

In the present study, we explored the interaction of MjTX-II and suramin using functional and structural approaches to advance knowledge regarding the structural basis for the mechanism of action of MjTX-II. A functional myographic study on a mice phrenic diaphragm preparation was performed to characterize the myotoxic effects of MjTX-II and its neutralization by suramin. The high-resolution crystal structure of the MjTX-II–suramin complex revealed interaction sites between the toxin and the ligand and its oligomeric conformation. Calorimetric assays were used to quantify the interactions between the protein inhibitors, and finally dynamic light-scattering and bioinformatics assays were performed to further evaluate the oligomeric characteristics of the complex.

## 2. Experimental procedures

### 2.1. Toxin isolation and suramin

MjTX-II was isolated from *B. moojeni* venom by ion-exchange chromatography using a gradient of 0.05–0.5 m*M* ammonium bicarbonate pH 8.0, as described previously (Soares *et al.*, 1998). Suramin sodium salt (catalogue No. S2671) was obtained from Sigma–Aldrich, St Louis, Missouri, USA.

### 2.2. Dynamic light scattering

Dynamic light-scattering (DLS) experiments were performed with a protein concentration of 2.5 mg ml$^{-1}$ for native MjTX-II and its complex with suramin (MjTX-II: suramin molar ratio of 1:10) using a DynaPro Titan device (Wyatt Technology) at 291 K. Measurements were performed with the protein dissolved in 50 m*M* ammonium bicarbonate pH 8.0, 50 m*M* sodium citrate pH 5.6. 100 measurements were acquired in each experiment. Analysis of the final data was performed with *DYNAMICS* v.6.10 (Wyatt Technology).

### 2.3. Isothermal titration calorimetry

MjTX-II–suramin isothermal titration calorimetric experiments were performed with an $iTC_{200}$ microcalorimeter (MicroCal, GE Healthcare). Titrations were performed in triplicate with the following general conditions: 2 µl injection volumes, a 240 s time spacing between injections, a stirring speed of 1000 rev min$^{-1}$, a reference differential power (DP) of 5 µcal s$^{-1}$, 45 µ*M* MjTX-II (in the reaction cell) and 600 µ*M* suramin (in the syringe). Assays were performed at 298 K in 50 m*M* ammonium bicarbonate buffer pH 8.0. Heats of dilution and mixing of suramin sodium salt were determined in separate control experiments and were subtracted from the titrations. Data analyses were performed using scripts based on binding polynomials implemented in *Origin* (v.7.0;

OriginLab, Northampton, Massachusetts, USA) as described previously (Freire *et al.*, 2009; Zhou *et al.*, 2008; Vega *et al.*, 2015).

### 2.4. Functional studies

*In vitro* neuromuscular studies were performed using a myographic technique in order to verify the influence of MjTX-II or its pre-incubation product with suramin upon the contractile process of isolated phrenic nerve–diaphragm muscle preparations of mice. Neuromuscular preparation has proven to be an invaluable tool in the examination of snake venoms and their components, since neuromuscular junctions and muscle fibres are the main target of action of these substances (for a review, see Hodgson & Wickramaratna, 2002). Diaphragm muscle can be stimulated either indirectly, by brief pulses in the motor nerve, or directly on the muscle. This allows discrimination between neurotoxic and myotoxic effects of a snake venom or toxin (Harvey *et al.*, 1994). While neurotoxicity only causes the loss of the indirect twitches, myotoxicity induces the depression of both direct and indirect twitches (Harvey *et al.*, 1994; Ownby *et al.*, 1999).

Adult male mice (25–30 g) were sacrificed by exsanguination after cervical dislocation. The phrenic nerve–muscle diaphragm preparations were removed and mounted vertically in a conventional, isolated organ-bath chamber containing 15 ml of a physiological solution with the following composition: 135 m*M* NaCl, 5 m*M* KCl, 2 m*M* $MgCl_2$, 15 m*M* $NaHCO_3$, 1 m*M* $Na_2HPO_4$, 11 m*M* glucose. This solution was bubbled with carbogen (95% $O_2$ and 5% $CO_2$) and maintained at 308 ± 1 K. The preparation was attached to an isometric force transducer (FT03, Grass Technologies) to record twitch tensions. The transducer signal output was amplified and recorded on a computer *via* a transducer signal conditioner (Part No. 13-6615-50, Gould) with an AcquireLab Data Acquisition System (Gould). The resting tension was 2 g. Indirect contractions were evoked by supramaximal pulses (0.2 Hz, 0.5 ms) delivered from an electronic stimulator (S88K, Grass Technologies) and applied to the phrenic nerve by means of a suction electrode. Direct contractions were evoked by supramaximal pulses (0.2 Hz, 5 ms) through a bipolar electrode positioned on opposite sides of the muscle. The direct contraction experiments were performed in the presence of pancuronium bromide ($2 \times 10^{-6}$ *M*). Preparations were allowed to stabilize for 45 min before the addition of MjTX-II (1 µ*M*) or of a mixture of MjTX-II plus suramin (10 µ*M*) pre-incubated at 308 K for 15 min. Animal procedures were in accordance with the guidelines for animal care prepared by the Committee on Care and Use of Laboratory Animal Resources, National Research Council, USA.

### 2.5. Crystallization and X-ray data collection

The purified MjTX-II fraction was concentrated to 10 mg ml$^{-1}$ in 0.05 m*M* ammonium bicarbonate pH 8.0 and suramin solution was added to give a 1:8 molar ratio. Crystals of the MjTX-II–suramin complex were obtained at 291 K from a mixture of 1 µl protein–suramin solution and 1 µl reservoir solution equilibrated against 500 µl reservoir solution [30%(*w*/*v*) PEG 4000, 0.1 *M* Tris–HCl pH 8.5, 0.2 *M* lithium sulfate] by the hanging-drop vapour-diffusion method (Ducruix & Giegé, 1992).

X-ray diffraction data were collected from a single MjTX-II–suramin crystal at a wavelength of 1.459 Å (at 100 K) using a synchrotron-radiation source [MX2 station, Laboratório Nacional de Luz Sincrotron (LNLS), Campinas, Brazil] and a MAR CCD imaging-plate detector (MAR Research). The crystal was mounted in a nylon loop and flash-cooled in a stream of nitrogen at 100 K without cryoprotectant. A crystal-to-detector distance of 100 mm and an oscillation range of 1° were used, resulting in the collection of 127 images. The data were processed to 1.9 Å resolution using the *HKL*-2000 program package (Otwinowski & Minor, 1997).

### 2.6. Structure determination and refinement

The crystal structure of the MjTX-II–suramin complex was solved by the molecular-replacement method using *Phaser* (McCoy, 2007) from the *PHENIX* package v.1.8.4 (Adams *et al.*, 2010) using the coordinates of MjTX-II (PDB entry 4kf3; Salvador, Cavalcante *et al.*, 2013) as the search model. The modelling process was performed by manual rebuilding using *Coot* v.0.7.1 (Emsley & Cowtan, 2004). Polyethylene glycol (PEG) 4000, water and suramin molecules were added by *Coot* and refined using the *PHENIX* package v.1.8.4 (Adams *et al.*, 2010). Because of a lack of electron density, the amino-acid side chains of Glu86 and Lys69 in monomer *A* and Lys128 in monomer *B* were not modelled. The *PHENIX* package and *MolProbity* (http://molprobity.biochem.duke.edu/; Chen *et al.*, 2010) were used to check the general quality of the final model. The coordinates were deposited in the PDB as entry 4yv5.

### 2.7. Comparative analysis

The structures of MjTX-II–suramin, MjTX-II (PDB entry 4kf3; Salvador, Cavalcante *et al.*, 2013), BaspTX-II–suramin (myotoxin II from *B. asper* venom; PDB entry 1y4l; Murakami *et al.*, 2005) and ecarpholin S–suramin (a myotoxic Ser49-$PLA_2$ from *Echis carinatus* venom; PDB entry 3bjw; Zhou *et al.*, 2008) were used. Molecular comparison of the structures was performed using *Coot* v.0.7.1 (Emsley & Cowtan, 2004). All structural figures were generated using *PyMOL* v.1.3 (Schrödinger).

### 2.8. Molecular-dynamics simulations

Molecular-dynamics (MD) simulations were performed using *GROMACS* (*Groningen Machine for Chemical Simulation*) v.4.5.3 (Van Der Spoel *et al.*, 2005) for two experimental conditions: four protomers of MjTX-II (a tetramer) without ligands and four protomers of MjTX-II (a tetramer) and four suramin molecules. The simulations were performed using the protein models in the presence of explicit water molecules. The GROMOS96 53a6 force field (Oostenbrink *et al.*, 2005) was selected to perform the MD simulations, and the protonation states of the charged groups were set to a pH

value of 7.0. The minimum distance between any atom of the models and the box wall was 0.5 nm. Energy minimization using a steepest-descent algorithm was performed to generate the starting configurations of the systems. After this step, 200 ps of MD simulation with positional restraints applied to the protein (PRMD) was executed to gently relax the systems. 50 ns of unrestrained MD simulation was then performed to evaluate the stabilities of the structures. All MD simulations were performed in a periodic truncated cubic box under constant temperature (298 K) and pressure (100 kPa), which were maintained by coupling to an isotropic pressure system and an external heat bath (van Gunsteren & Berendsen, 1984). The suramin topology and coordinate files used in the MD simulations were generated by the *PRODRG*2.5 server at the University of Dundee (http://davapc1.bioch.dundee.ac.uk/cgi-bin/prodrg).

The overall stereochemistry and fold quality of the protein structural models obtained after initial modelling and MD simulations were further examined with *RAMPAGE* (Lovell *et al.*, 2003) and *ProSA-web* (Wiederstein & Sippl, 2007). To assess the quality of the MD simulations, the average root-mean-square deviation/time graphs of the protein backbone atoms were analyzed to examine the differences between the total averages of two equal sets of points (the points corresponding to the transient part of the simulations were not considered).

## 3. Results

### 3.1. *In vitro* myotoxicity

MjTX-II at 1 µ*M* promoted a time-dependent blockade of both indirectly and directly evoked twitches in mouse neuromuscular preparations (Fig. 1). Pre-incubation with suramin prevented approximately 85% of the muscle paralysis promoted by MjTX-II, independent of whether the stimulus was applied directly into the muscle or indirectly into the nerve. Suramin alone did not alter muscle contractions compared with the control.

### 3.2. Dynamic light scattering

DLS experiments were performed using the toxin dissolved in ammonium bicarbonate pH 8.0 and sodium citrate pH 5.6. An $R_h$ value of 2.0 nm was obtained in both conditions, with polydispersivity values of Pd = 9.5% at pH 5.6 and Pd = 13.9% at pH 8. An average molecular weight of approximately 17 kDa was calculated considering MjTX-II to be a globular protein (the sequence-based monomeric molecular weight is 13.887 kDa). A similar value was obtained ($R_h$ = 2.3 Å, Pd = 12%) for native MjTX-II dissolved in ultrapure water, as described previously (Salvador, Cavalcante *et al.*, 2013). These results are also consistent with data obtained previously for other Lys49-PLA$_2$s (Fernandes *et al.*, 2010). Thus, taking into account that the structure is not perfectly globular, the data suggest that native MjTX-II is predominantly dimeric, but the presence of a fraction of the toxin in a monomeric conformation may also be possible. Conversely, DLS measurements of pre-incubated MjTX-II–suramin solution indicated protein oligomerization ($R_h$ = 4.2 nm, Pd = 13.7% at pH 5.6 and $R_h$ = 3.5 nm, Pd = 14.5% at pH 8). The calculated molecular weight of the complex is 98 and 63 kDa at pH 5.6 and 8.0, respectively. These data clearly demonstrated the oligomerization process undergone by the complex, and also suggest that the tetramer is the predominant assembly for the complex at pH 8.0, despite the relatively high polydispersivity value in these measurements.

### 3.3. Interaction between MjTX-II and suramin

The interaction between MjTX-II and suramin was assessed by ITC. A representative calorimetric titration is shown in Fig. 2. The thermogram exhibited biphasic behaviour, indicating at least two distinguishable binding events. To avoid *a priori* constraints regarding the ligand-binding sites, a general

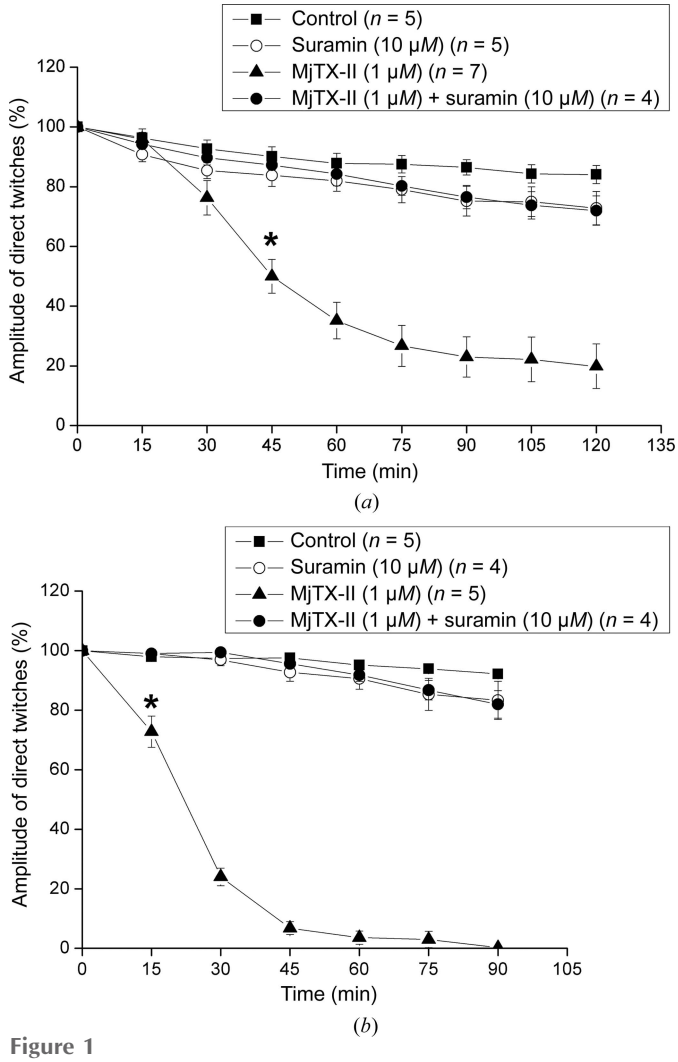


**Figure 1**
Effects of MjTX-II and the product of its pre-incubation with suramin on (*a*) directly and (*b*) indirectly evoked twitches in mouse phrenic diaphragm preparations. The ordinate represents the percentage of twitches relative to the initial amplitude. The abscissa indicates the time (in minutes) after the addition of MjTX-II or a mixture of MjTX-II and suramin to the organ bath. The data are grouped as means ± standard error of the mean ($P < 0.05$). The asterisk indicates the point after which there was a significant difference compared with the control.

**Table 1**
Thermodynamic values for the binding of suramin to MjTX-II.

$k_{d1}$ and $k_{d2}$ are the intrinsic dissociation constants for the binding of the first and second ligand. $\Delta h_1$ and $\Delta h_2$ are the intrinsic binding enthalpies for the binding of the first and second ligand. $\beta_1$ and $\beta_2$ are the overall association constants for the first and second binding events. $\Delta H_1$ and $\Delta H_2$ are the overall binding enthalpies for the first and second binding events. $\alpha$ is the interaction cooperativity constant ($= 4\beta_2/\beta_1^2$). $\Delta h$ is the interaction cooperativity enthalpy. $n_H$ is the Hill coefficient [$= 2/(1 + \alpha^{-1/2})$].

| | |
|---|---|
| Dissociation binding constants and binding enthalpies | |
| $k_{d1}$ ($\mu M$) | $0.6 \pm 0.1$ |
| $\Delta h_1$ (kcal mol$^{-1}$) | $5.2 \pm 0.2$ |
| $k_{d2}$ ($\mu M$) | $6.2 \pm 1.2$ |
| $\Delta h_2$ (kcal mol$^{-1}$) | $-18.2 \pm 0.6$ |
| Overall binding parameters determined by nonlinear regression | |
| $\beta_1$ ($M^{-1}$) | $(3.1 \pm 0.5) \times 10^6$ |
| $\Delta H_1$ (kcal mol$^{-1}$) | $5.2 \pm 0.3$ |
| $\beta_2$ ($M^{-2}$) | $(2.5 \pm 0.4) \times 10^{11}$ |
| $\Delta H_2$ (kcal mol$^{-1}$) | $-13.0 \pm 0.3$ |
| $\alpha$ | $0.10 \pm 0.03$ |
| $\Delta h$ (kcal mol$^{-1}$) | $-23.4 \pm 0.4$ |
| $n_H$ | $0.5 \pm 0.2$ |

**Table 2**
X-ray data-collection and refinement statistics.

Values in parentheses are for the highest resolution shell.

| | |
|---|---|
| Unit-cell parameters (Å) | $a = 50.8$, $b = 63.6$, $c = 87.7$ |
| Space group | $P2_12_12_1$ |
| Resolution (Å) | 31.82–1.90 (1.96–1.90) |
| Unique reflections | 23031 (2258) |
| Completeness (%) | 99.9 (99.7) |
| $\langle I/\sigma(I)\rangle$ | 8.6 (2.5) |
| Multiplicity | 4.9 (4.7) |
| Molecules in asymmetric unit | 2 |
| $R_{merge}$† (%) | 14.4 (78.9) |
| $R_{cryst}$ (%) | 19.7 |
| $R_{free}$ (%) | 22.8 |
| No. of non-H atoms | |
| Protein | 1916 |
| Waters | 197 |
| Suramin molecules | 2 |
| PEG 4K molecules | 3 |
| Sulfate ions | 7 |
| Wilson $B$ factor (Å$^2$) | 20.6 |
| Ramachandran plot‡ (%) | |
| Favoured | 95.0 |
| Outliers | 0.91 |

† $R_{merge} = \sum_{hkl}\sum_i |I_i(hkl) - \langle I(hkl)\rangle| / \sum_{hkl}\sum_i I_i(hkl)$, where $I_i(hkl)$ is the intensity of an individual measurement of the reflection with Miller indices $hkl$ and $\langle I(hkl)\rangle$ is the mean intensity of that reflection. Calculated for $I > -3\sigma(I)$. ‡ Calculated with *MolProbity* (Chen *et al.*, 2010).

model with two binding sites based on the overall association constants ($\beta_1$ and $\beta_2$) and binding enthalpies ($\Delta H_1$ and $\Delta H_2$) was employed. Nonlinear regression analysis allowed the estimation of binding parameters (Table 1). An interaction constant $\alpha$ ($= 4\beta_2/\beta_1^2$) of 0.1 and a Hill coefficient of 0.5 indicated that the binding sites are either non-identical or identical exhibiting negative cooperativity.

Intrinsic site-specific binding parameters were calculated from the overall association parameters: the dissociation constants for the binding of the first and second events and their corresponding binding enthalpies (Table 1). The first binding event presented a dissociation constant of 0.6 $\mu M$, whereas the second binding event displayed a dissociation constant of 6.2 $\mu M$ (a tenfold reduction in binding affinity). There was a considerable difference in the binding enthalpies: the first event exhibited unfavourable enthalpy (entropically driven), whereas the second event exhibited favourable enthalpy (enthalpically driven, with a $-23.4$ kcal mol$^{-1}$ difference in enthalpy).

### 3.4. Crystallographic structure of the MjTX-II–suramin complex

The MjTX-II–suramin crystals belonged to space group $P2_12_12_1$ and diffracted to 1.9 Å resolution. The refinement converged to an $R_{cryst}$ value of 19.7% ($R_{free}$ = 22.8%) with a final model (Fig. 3*a*) composed of 197 solvent molecules, two suramin molecules (Fig. 3*b*), seven sulfate ions and three polyethylene glycol 4000 (PEG 4K) molecules. This model revealed two protomers (identified as *A* and *B*) in the asymmetric unit. The refinement statistics and other information are provided in Table 2. Suramin molecules bind to both monomers of the MjTX-II–suramin complex in a symmetric manner, establishing interactions with both the C- and N-termini of the toxin (the Lys7, Leu10, Asn114, Lys116, Tyr119, Tyr121, Leu122 and Phe126 residues are involved in these interactions; Figs. 4*a* and 4*b*).

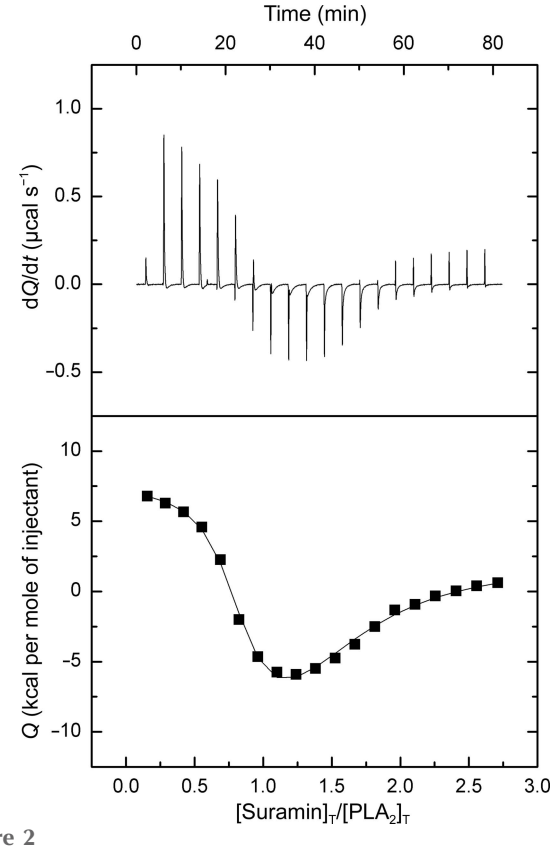


**Figure 2**
Calorimetric titration of suramin sodium salt into MjTX-II. The upper panel shows the raw data thermogram (thermal power as a function of time) of the titration of MjTX-II (200 µl, 45 $\mu M$) with 600 $\mu M$ suramin sodium salt. The lower panel shows the binding isotherm (ligand-normalized integrated heat as a function of the molar ratio). Affinities and enthalpy changes were determined by a general nonlinear regression model considering two ligand-binding sites (solid line).

The crystallographic structure of MjTX-II complexed with suramin presents a similar fold to other class II $PLA_2$s, is stabilized by seven disulfide bridges and is composed of the following secondary-structure elements: an N-terminal $\alpha$-helix (h1), a 'short' helix, a $Ca^{2+}$-binding loop, two antiparallel $\alpha$-helices (h2 and h3), two short strands of antiparallel $\beta$-sheets (known as $\beta$-wings) and a C-terminal loop (Arni & Ward, 1996; Magro *et al.*, 2009). The MjTX-II–suramin structure, like other $PLA_2$-like structures, presents a hydrophobic channel which links the protein surface to its putative active site. This cleft is present for both catalytic $PLA_2$s and $PLA_2$-like proteins, displaying conserved residues (*e.g.* His48) that are fundamental for the catalytic process (in $PLA_2$s; Scott & Sigler, 1994) or for the mechanism of toxicity (in $PLA_2$-like proteins; dos Santos *et al.*, 2009).

The majority of $PLA_2$-like toxins present dimeric arrangements in their crystals and in solution (Fernandes *et al.*, 2014). Additionally, the unit-cell packing of MjTX-II–suramin and most Lys49-$PLA_2$ structures presents two possible dimeric configurations: (i) the 'alternative dimer' or 'compact dimer' and (ii) the 'conventional dimer' or 'larger dimer'. This issue has been extensively analyzed in different studies, with the 'alternative dimer' being the most likely conformation to occur in solution (for a review, see Fernandes *et al.*, 2014). Inspection of the MjTX-II–suramin unit-cell packing using *PISA* (Krissinel & Henrick, 2007) also suggested that the 'alternative dimer' conformation is the most probable conformation to occur in solution: the 'alternative dimer' had a complexation signification score (CSS) of 0.2, an interfacial area of 512.5 $Å^2$ and $\Delta^i G = -9.4$ kcal $mol^{-1}$, while the 'conventional dimer' had a CSS of 0, an interfacial area of 348.2 $Å^2$ and $\Delta^i G = -0.2$ kcal $mol^{-1}$. Thus, the first assembly (alternative dimer) was selected for the MjTX-II–suramin structure and used in refinement.

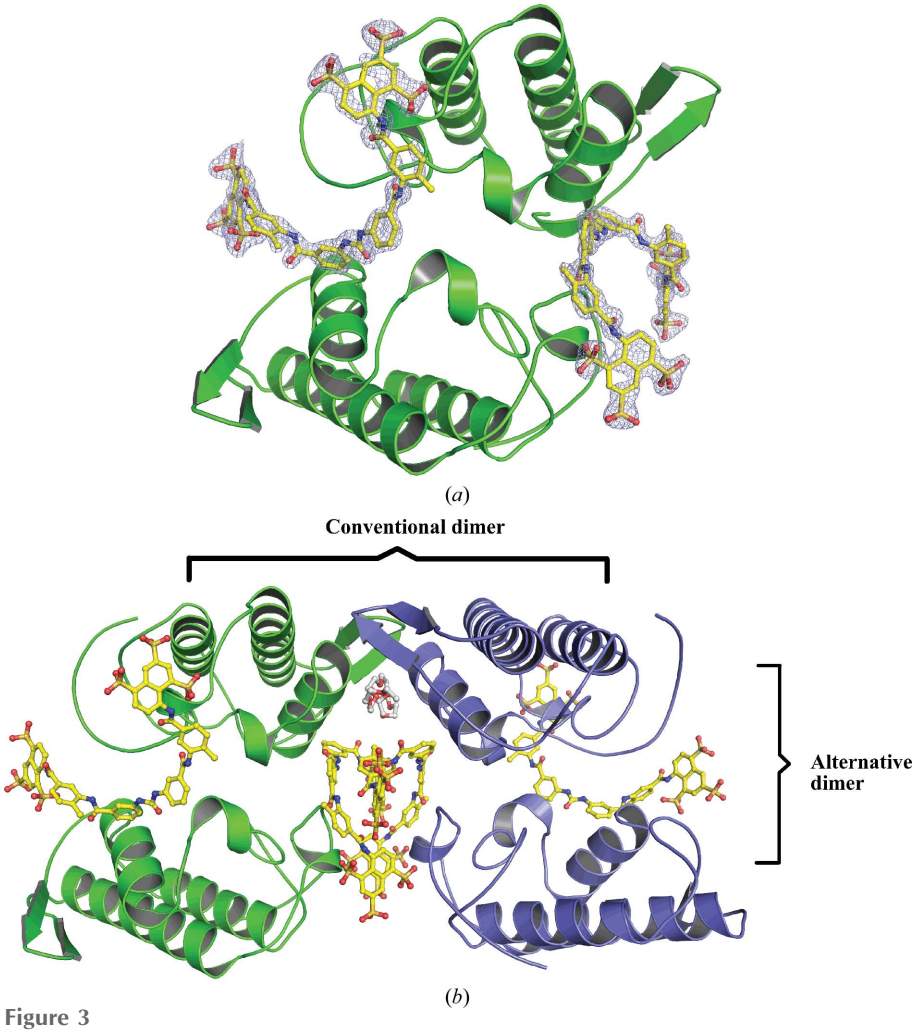


**Figure 3**
Crystal structure of the MjTX-II–suramin complex. (*a*) The overall structure of the MjTX-II–suramin complex is depicted as a ribbon diagram. Suramin molecules (yellow) are illustrated as stick representations. The electron-density map (coefficients $|F_{obs}| - |F_{calc}|$) of the MjTX-II–suramin complex is shown in the area corresponding to the ligand and is contoured at 1.0$\sigma$. (*b*) Tetrameric configuration of the MjTX-II–suramin complex formed by two dimers in the asymmetric unit. This oligomeric conformation was suggested by *PISA* (Krissinel & Henrick, 2007), dynamic light scattering and molecular-dynamics simulations to be stable in solution. Both 'alternative' and 'conventional' dimers were observed in this oligomeric conformation (Fernandes *et al.*, 2014).

The particular mode of suramin binding on the toxin surface, in which there is a ligand on each side of the dimer (Fig. 3*a*), enables other toxin dimers to interact with each side of the complex, allowing higher-order complex formation (Fig. 3*c*). Notably, this oligomeric organization of the MjTX-II–suramin complex is composed of four protomers that are composed of two dimers in the 'alternative dimer' conformation (from two asymmetric units) related by a twofold axis. The majority of the contacts between the dimers are between two suramin molecules that are located in the dimeric interface (Fig. 3*c*). Further analyses with *PISA* (using the protomers, suramin and the interfacial PEG 4K molecules) suggested a tetrameric conformation as a stable assembly in solution. Another interesting feature that is observed in the tetrameric arrangement is the presence of both 'alternative' and 'conventional' dimers (Fig. 3*c*). Thus, despite the 'alternative' conformation being more favourable in solution for most Lys49-$PLA_2$s, the 'conventional' conformation is found in the case of a tetrameric arrangement, such as in MjTX-II–suramin and MjTX-I (Salvador, Fernandes *et al.*, 2013).

### 3.5. Comparison between MjTX-II and the MjTX-II–suramin complex

MjTX-II and the MjTX-II–suramin complex displayed similar dimeric structures (r.m.s.d. of 0.33 Å). The main differences between these structural

models are observed in the ligand-binding regions (Figs. 5*b* and 5*d*). The MjTX-II structure contains four PEG 4K molecules: the PEG 4K(1) and PEG 4K(2) molecules inside the hydrophobic channel of each dimer, PEG 4K(3) interacting with the Lys7 region and PEG 4K(4) interacting with the hydrophobic channels of both monomers simultaneously (each tail is bound to each monomer). In the MjTX-II–suramin complex there are only three PEG 4K molecules [the PEG 4K(4) molecule is absent]. Additionally, the PEG 4K(3) molecule observed in the vicinity of the Lys7 residue presents a different configuration compared with that observed in the MjTX-II structure. Part of this PEG 4K molecule interacts with one of the monomers of the adjacent dimer of the asymmetric unit of the MjTX-II–suramin structure (Fig. 3*a*). Finally, the most important characteristic of the complex is the presence of two suramin molecules on the surface of the toxin dimer. This particular binding mode of the ligands on the protein surface creates the possibility of the occurrence of a high-order oligomeric assembly.

### 3.6. Comparison between $PLA_2$-like toxins complexed with suramin

Three structures of $PLA_2$-like toxins complexed with suramin have been solved: (i) MjTX-II–suramin (this work), (ii) BaspTX-II–suramin (a Lys49-$PLA_2$ from *B. asper*; Murakami *et al.*, 2005) and (iii) ecarpholin S–suramin (a Ser49-$PLA_2$ from *E. carinatus*; Zhou *et al.*, 2008). Notably, the ligand binds to different parts of each protein, leading to different oligomeric conformations of the toxins.

A comparison between the crystal structures of the two Lys49-$PLA_2$s complexed with suramin (MjTX-II–suramin and BaspTX-II–suramin) in their dimeric arrangement is shown in Fig. 5(*a*). The structure of the BaspTX-II–suramin complex demonstrated that suramin interacts with the putative calcium-binding loop and C-terminal regions. The ligand is bound at the entrance to the hydrophobic channel of the toxin, blocking the access to a possible activator molecule (see §4.3). In MjTX-II–suramin, by contrast, the inhibitor is bound at the external portion of the protein in both monomers (Fig. 3*a*) by several hydrophobic contacts and three polar contacts (Figs. 4*a* and 4*b*). This particular mode of interaction also results in oligomerization of the complex, mainly by contacts between the suramin molecules. The reasons for the ligand-binding differences between these two proteins arise from two unique sequence features of MjTX-II compared with all other Lys49-$PLA_2$s (Salvador, Cavalcante *et al.*, 2013): (i) a mutation in the putative $Ca^{2+}$-binding loop (Leu32Gly) causes the binding of the additional PEG 4K(4) molecule (Fig. 5*d*) in the structure of MjTX-II–PEG 4K and of an additional fatty-acid

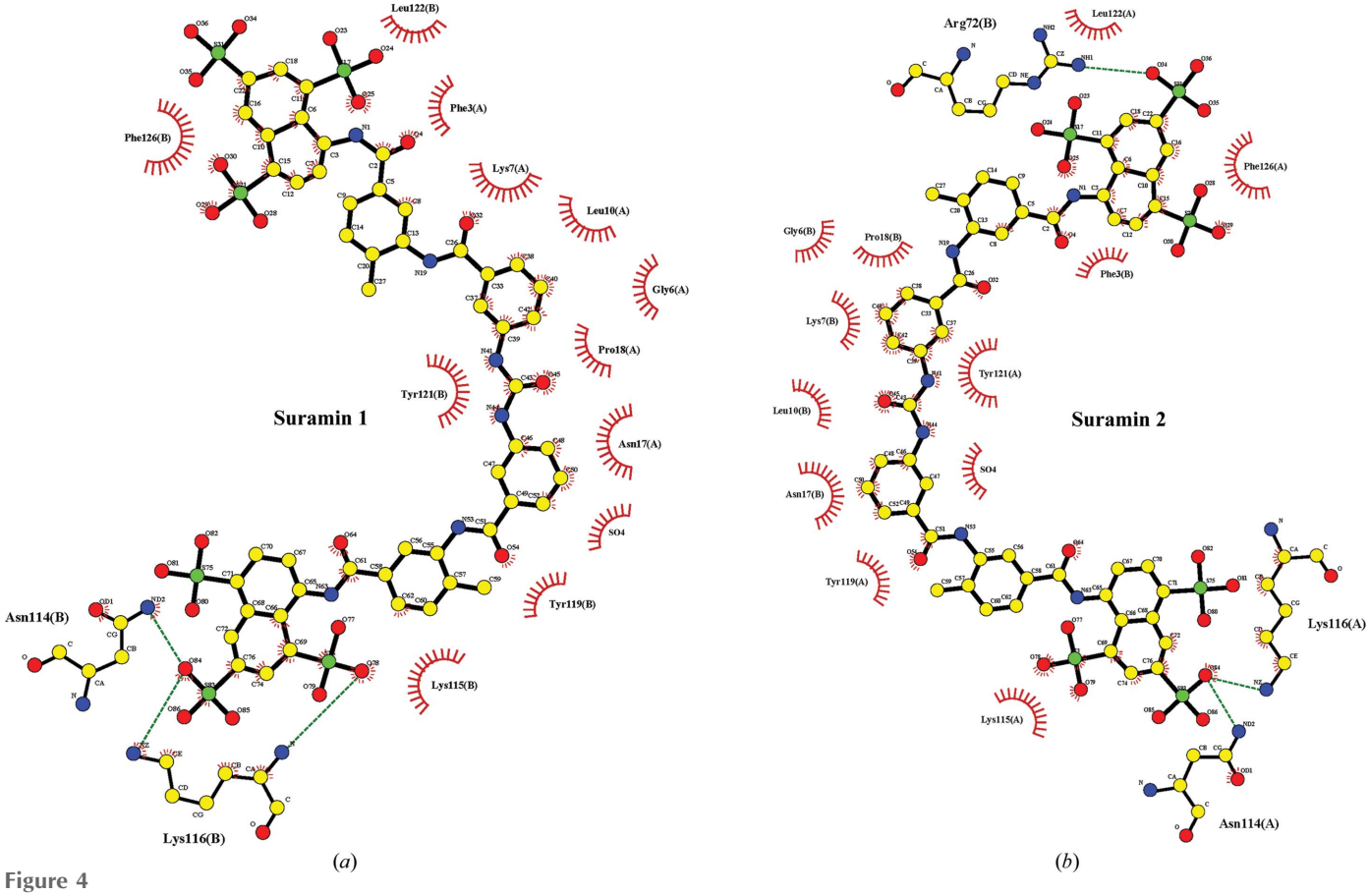


**Figure 4**
Interaction of suramin molecules in the MjTX-II structure. (*a*) and (*b*) represent the interactions of suramin 1 and suramin 2 bound to monomers *A* and *B* of MjTX-II, respectively. Polar contacts are depicted as broken lines and hydrophobic contacts are indicated by arcs with radiating spokes. This figure was drawn using *LIGPLOT* (Wallace *et al.*, 1995).

molecule in the structure of MjTX-II–stearic acid (Watanabe *et al.*, 2005) and (ii) an insertion in the MjTX-II C-terminus (Asn120) also confers a different conformation to this region, leading to the binding of the additional PEG 4K(3) (Fig. 5*d*) in the MjTX-II–PEG 4K structure or a fatty-acid molecule in the MjTX-II–stearic acid structure (Salvador, Cavalcante *et al.*, 2013; Watanabe *et al.*, 2005). Indeed, phylogenetic studies with $PLA_2$-like toxins demonstrated that the MjTX-II sequence is in an isolated and primitive branch of the Lys49-$PLA_2$ clade (dos Santos, Cintra-Francischinelli *et al.*, 2011; Salvador, Fernandes *et al.*, 2013).

A superposition of the MjTX-II–suramin and ecarpholin S–suramin (Zhou *et al.*, 2008) dimers is shown in Fig. 6. It can be observed that although they present a conserved secondary structure, their oligomeric structures are very different and the C-terminal regions also display different conformations. The ecarpholin S–suramin crystal structure contained three suramin ligands interacting with different portions of C-terminal and N-terminal regions of the toxin mainly by polar contacts. Interestingly, despite structural and sequential differences between the toxins (MjTX-II and ecarpholin S), some parts of the suramin ligands bind to similar regions (the C-terminal and N-terminal portions), and interaction between the ligands resulted in the oligomerization of both proteins.

### 3.7. Molecular-dynamics studies

MD simulations were performed to check the stability of the tetrameric structure of the complex observed in the unit cell. Thus, two different models were used for the MD simu-

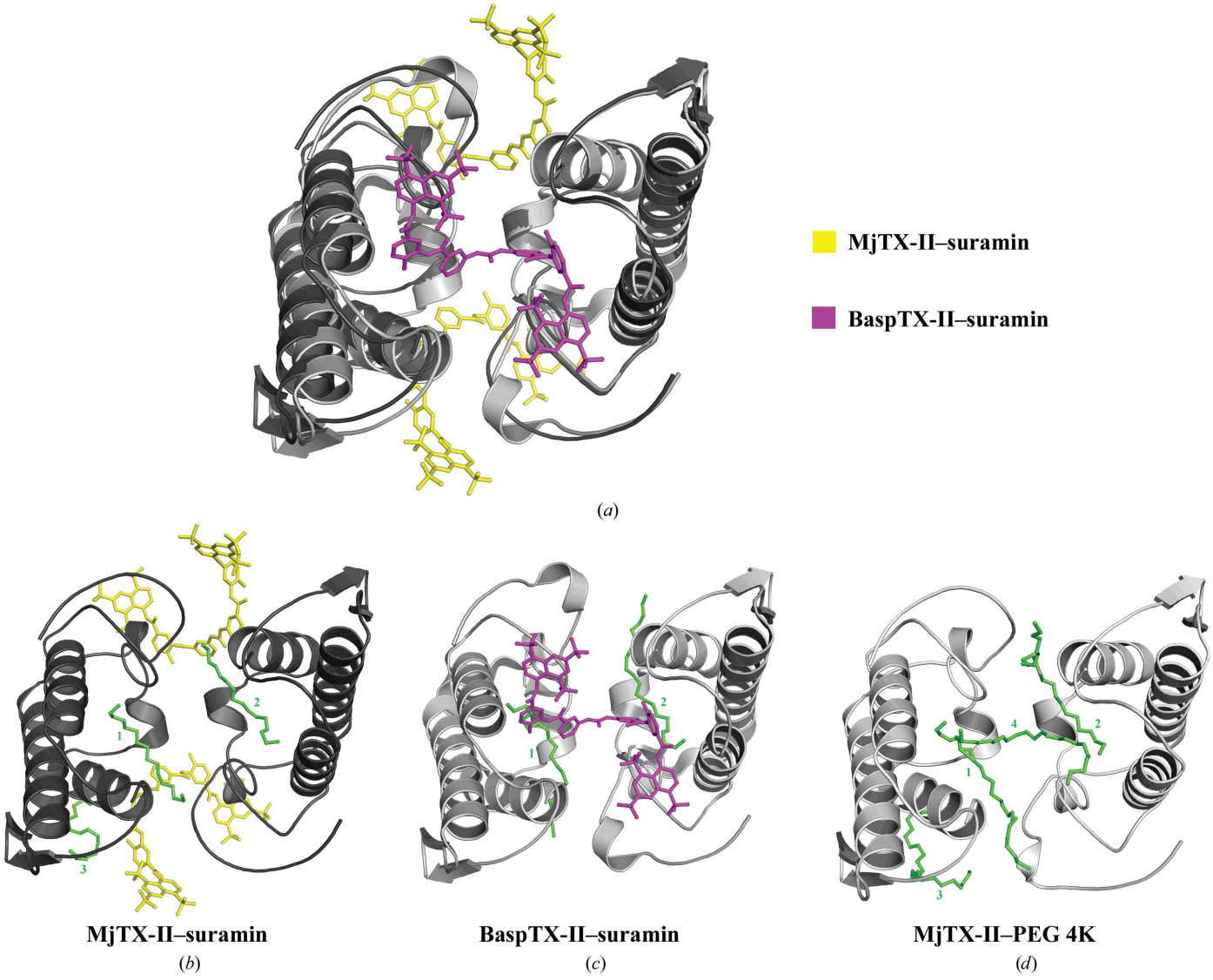


**Figure 5**
Structural comparison between the dimeric MjTX-II–suramin complex structure and other Lys49-$PLA_2$ structures. (*a*) Superposition of the MjTX-II–suramin (ribbon diagram in black and suramin molecules in yellow) and BaspTX-II–suramin (ribbon diagram in grey and suramin molecules in magenta) structures. (*b*) Cartoon representation of the dimeric MjTX-II–suramin complex structure (black); the three PEG 4K molecules and two suramin molexules are shown in green and yellow, respectively. (*c*) Cartoon representation of the BaspTX-II–suramin complex structure (grey); the two PEG 4K molecules are shown in green and the two suramin molecules are shown in magenta. (*d*) Cartoon representation of the MjTX-II structure (grey) with its four PEG 4K molecules shown in green.

lations: (i) a crystallographic tetrameric assembly of the complex (four protomers and four interfacial suramin molecules, named the bound assembly) and (ii) a crystallographic tetrameric assembly without suramin ligands (four protomers, named the unbound assembly).

The simulations showed that the bound assembly had a lower average r.m.s.d. value and also a lower level of r.m.s.d. fluctuations compared with the unbound assembly (Fig. 7). Thus, these data showed that the bound tetrameric assembly presented a lower tendency for movement between the dimers along the tetrameric interface, indicating tight interactions between the suramin molecules and toxin protomers.

## 4. Discussion

### 4.1. Myotoxic activity of MjTX-II is neutralized by suramin

Functional myographic studies performed on isolated neuromuscular preparations are suitable for screening the neurotoxic and myotoxic components of snake venoms (Gallacci & Cavalcante, 2010; Harvey *et al.*, 1994; Ownby *et al.*, 1999). Although neurotoxic activity is characterized by the exclusive blockade of indirect contractions, myotoxicity causes a loss of both direct and indirect twitches (Ownby *et al.*, 1999). The present study demonstrates that MjTX-II, similar to other Lys49-$PLA_2$s, induces a blockade of both indirect and direct twitches in mouse phrenic diaphragm preparations (Cavalcante *et al.*, 2005; de Oliveira *et al.*, 2003; Gallacci *et al.*, 2006; Heluany *et al.*, 1992; Oshima-Franco *et al.*, 2004; Ponce-Soto *et al.*, 2009; Randazzo-Moura *et al.*, 2008; Rodrigues *et al.*, 2004; Salvador, Fernandes *et al.*, 2013; Salvador, Cavalcante *et al.*, 2013; Soares *et al.*, 2001; Stábeli *et al.*, 2006). The muscle paralysis induced by myotoxic $PLA_2$s has been attributed to muscle-fibre unexcitability consequent to prolonged depolarization resulting from the alteration of cell-membrane permeability. Even though morphological studies clearly demonstrate that Lys49-$PLA_2$s can induce muscle damage, functional myographic approaches reveal the early stages of this toxic effect (de Oliveira *et al.*, 2003; Cavalcante *et al.*, 2007; dos Santos, Cardoso *et al.*, 2011).

As described above, pre-incubation with suramin neutralizes the muscle paralysis promoted by MjTX-II in mouse phrenic nerve–diaphragm preparations, regardless of whether the stimulus was applied indirectly on the nerve or directly on the muscle. Thus, based on the above considerations, we suggest that suramin neutralizes the myotoxic effect of MjTX-II. Similar findings regarding the antimyotoxic effect of suramin have previously been described against other $PLA_2$-like proteins, such as Lys49-$PLA_2$s [BthTX-I from *B. jararacussu* (de Oliveira *et al.*, 2003), BaspTX-II (Murakami *et al.*, 2005)] and ecarpholin S (Zhou *et al.*, 2008).

The mechanism of action of suramin at the neuromuscular junction remains unclear, but it is known that suramin blockades presynaptic voltage-dependent $Ca^{2+}$channels on the motor nerve terminal, reducing the release of acetylcholine (Henning *et al.*, 1996; Lin *et al.*, 2000). However, this mode of

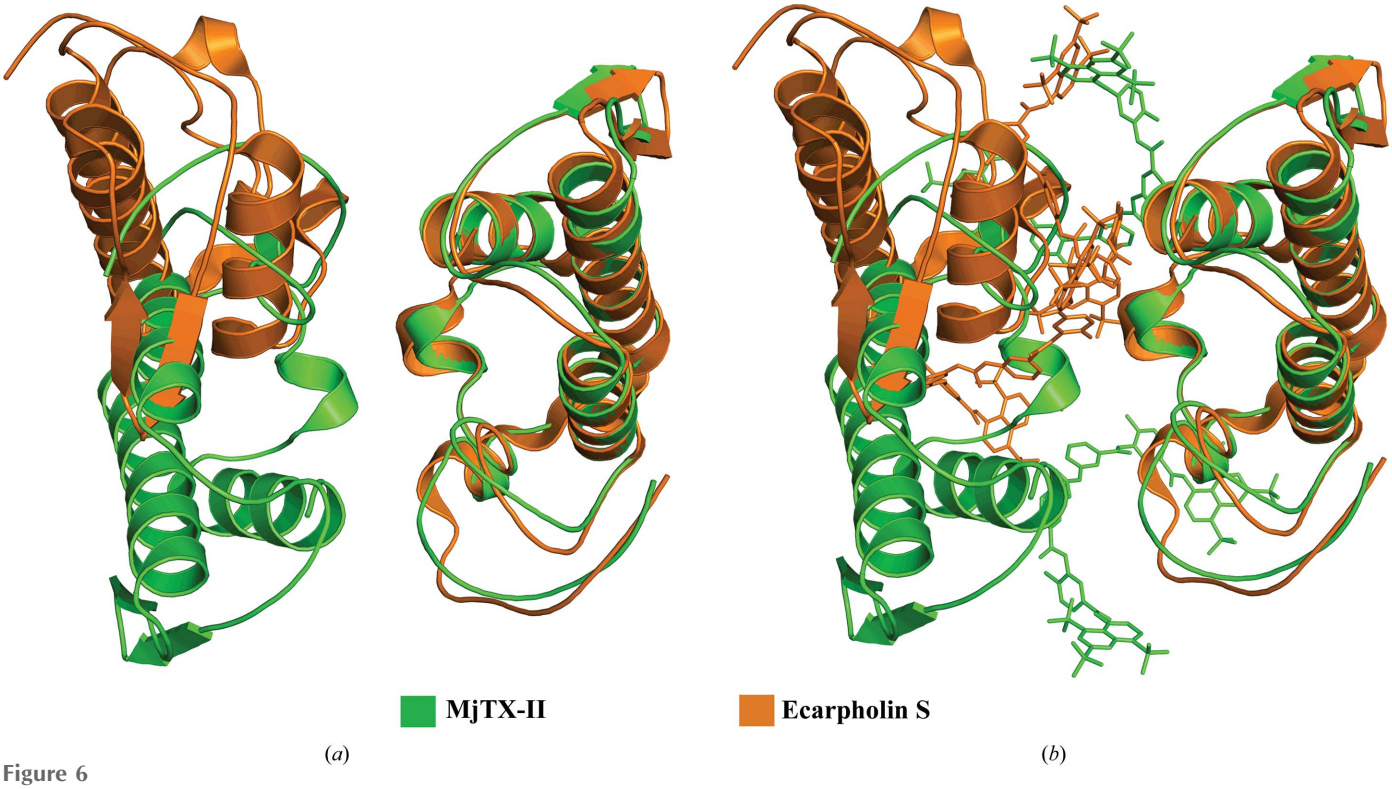


**Figure 6**
Superposition of the dimeric MjTX-II–suramin and the Ser49-$PLA_2$ escarpholin S–suramin structures. (*a*) Cartoon representation of the MjTX-II–suramin (green) and escarpholin S–suramin (light brown) structures. (*b*) The same superposition as in (*a*) but including the suramin molecules. One monomer of each structure was superposed to illustrate the oligomeric differences between the complexes.

action cannot account for the inhibitory effect of suramin on muscle paralysis induced by MjTX-II and other $PLA_2$-like toxins. Indeed, these functional results also corroborate our crystallographic and calorimetric assay results, indicating that suramin can interact with MjTX-II with high affinity and form complexes that are inactive.

### 4.2. Oligomerization of the MjTX-II–suramin complex

Most apo and complexed $PLA_2$-like structures are dimeric, as demonstrated by crystallography, DLS, SAXS and size-exclusion chromatography, among other techniques (Murakami *et al.*, 2007; dos Santos *et al.*, 2009; Fernandes *et al.*, 2010, 2014). In particular, the crystal structure of MjTX-II was also solved as a dimer (de Azevedo *et al.*, 1997; Watanabe *et al.*, 2005; Salvador, Cavalcante *et al.*, 2013). The MjTX-II–suramin structure also presents a dimeric conformation in its asymmetric unit; however, analysis of its unit cell shows that owing to crystallographic symmetry the tetrameric conformation seems to be most likely to occur. Notably, the dimeric conformation observed in the MjTX-II structure is also preserved in the MjTX-II–suramin structure. However, because the ligand binds on the surface of the toxin, a tetrameric arrangement formed by two dimers occurs in the unit cell.

To test whether the tetrameric arrangement occurs in solution, we also performed other experiments which, despite the particularities and limitations of each technique, demonstrated that a high-order oligomeric conformation is feasible. MD simulations demonstrated that the tetrameric conformation is more stable in the presence of the ligand. DLS assays indicated that the presence of the ligand induces the formation of higher-order oligomers, and also suggested that the tetrameric assembly is predominant at pH 8. ITC experiments indicated two binding events characterized by dissociation constants in the low micromolar range with a tenfold difference. Thus, these two events may be attributed to binding of suramin to the surface of MjTX-II (the first event with a higher dissociation constant, with positive enthalpy and entropically driven) and the interaction between the two dimers (by suramin and $\beta$-sheet residues) forming the tetrameric arrangement (the second event with a lower dissociation constant and enthalpically driven).

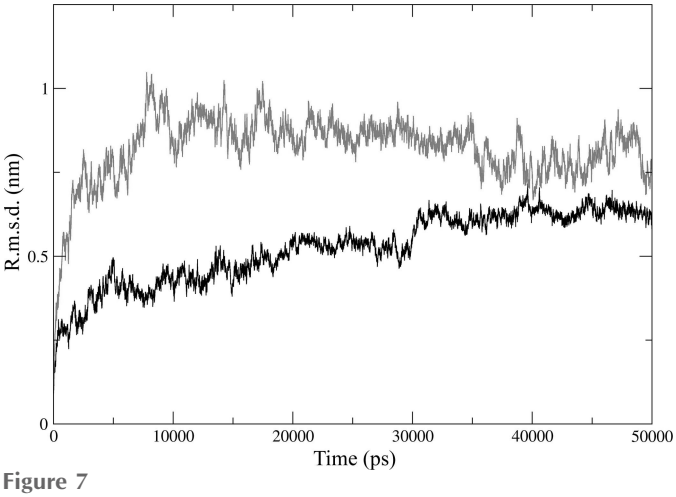


**Figure 7**
Average backbone r.m.s.d. during 50 ns molecular-dynamic simulations of the tetrameric assembly of MjTX-II with (black) and without (grey) suramin ligands. The simulations demonstrated that the bound assembly (in black) presents a lower average r.m.s.d. value and a lower level of r.m.s.d. fluctuations compared with the unbound assembly (grey).

Suramin-induced oligomerization has also been reported for ecarpholin S, a Ser49-$PLA_2$ from *E. carinatus* venom (Zhou *et al.*, 2008). The myotoxic activity of ecarpholin S is significantly inhibited by suramin, and oligomerization may be essential for this inhibition: the apo form of this protein changed from a monomeric to a dimeric state (in the asymmetric unit) and an octameric conformation (in the unit cell) when in the presence of suramin (Zhou *et al.*, 2008). Thus, considering the crystallographic and biophysical experiments, in which we showed that the oligomerization process also occurs for MjTX-II, we suggest that this phenomenon may also play an important role in the mechanism of inhibition of $PLA_2$-like toxins by suramin.

### 4.3. Structural basis for the inhibition of MjTX-II by suramin

The mechanism of action of Lys49-$PLA_2$s upon muscle fibres has been much discussed over the last several years, and great progress has been achieved regarding this topic. It is already known that Lys49-$PLA_2$s act as dimers through their C-terminal region (Chioato *et al.*, 2002; Ward *et al.*, 2002). It has been proposed that C-terminal (Lys115 and Arg118) and other basic residues (such as Lys20) are the main residues responsible for membrane anchorage (dos Santos *et al.*, 2009). More recently, this anchorage site was named the membrane-docking site (MDoS) and other functional sites responsible for membrane disruption (called membrane-disruption sites; MDiS) consisting of the C-terminal hydrophobic residues (Leu121 and Phe125 in Lys49-$PLA_2$s and Leu122 and Phe126 in MjTX-II because of a residue insertion) have been identified (Fernandes *et al.*, 2013). Thus, a myotoxic mechanism composed of five steps was proposed: (i) fatty-acid binding at the hydrophobic channel of the toxin, (ii) allosteric activation, (iii) protein–membrane docking (MDoS), (iv) protein penetration and disruption (MDiS) and (v) cell death (Fernandes *et al.*, 2013).

Based on the available structural and functional data, different 'classes' of inhibitors of $PLA_2$-like proteins have been proposed: (i) ligands that bind in the hydrophobic channel (*e.g. p*-bromophenacyl bromide; BPB), (ii) ligands that block or restrict access to the hydrophobic channel (*e.g.* rosmarinic acid) and (iii) ligands that bind to the C-terminus or the MDoS (dos Santos *et al.*, 2009; Fernandes *et al.*, 2014). Notably, the crystal structure of the MjTX-II–suramin complex shows that suramin binds simultaneously to the MDoS and MDiS regions (primarily localized at the C-termini of $PLA_2$-like toxins; Figs. 4 and 8). Suramin simultaneously neutralizes the myotoxic and neuromuscular blocking activity of MjTX-II when pre-incubated *in vitro*. Calorimetric data demonstrated that suramin ligands bind to MjTX-II in the low micromolar range, which corroborates the functional data.

Thus, the interaction of suramin with MjTX-II is in agreement with the previous hypothesis for class (iii) inhibitors (C-termini) but also reveals a broader class of inhibitor that is able to bind to both the MDiS and MDoS regions. This is the first report of a ligand that binds simultaneously to both sites and explains its high efficiency as an inhibitor, as demonstrated by functional and calorimetric assays.

In addition to suramin binding at the MDiS and MDoS regions of MjTX-II, the oligomerization process observed for the MjTX-II–suramin complex also strengthens the MDiS and

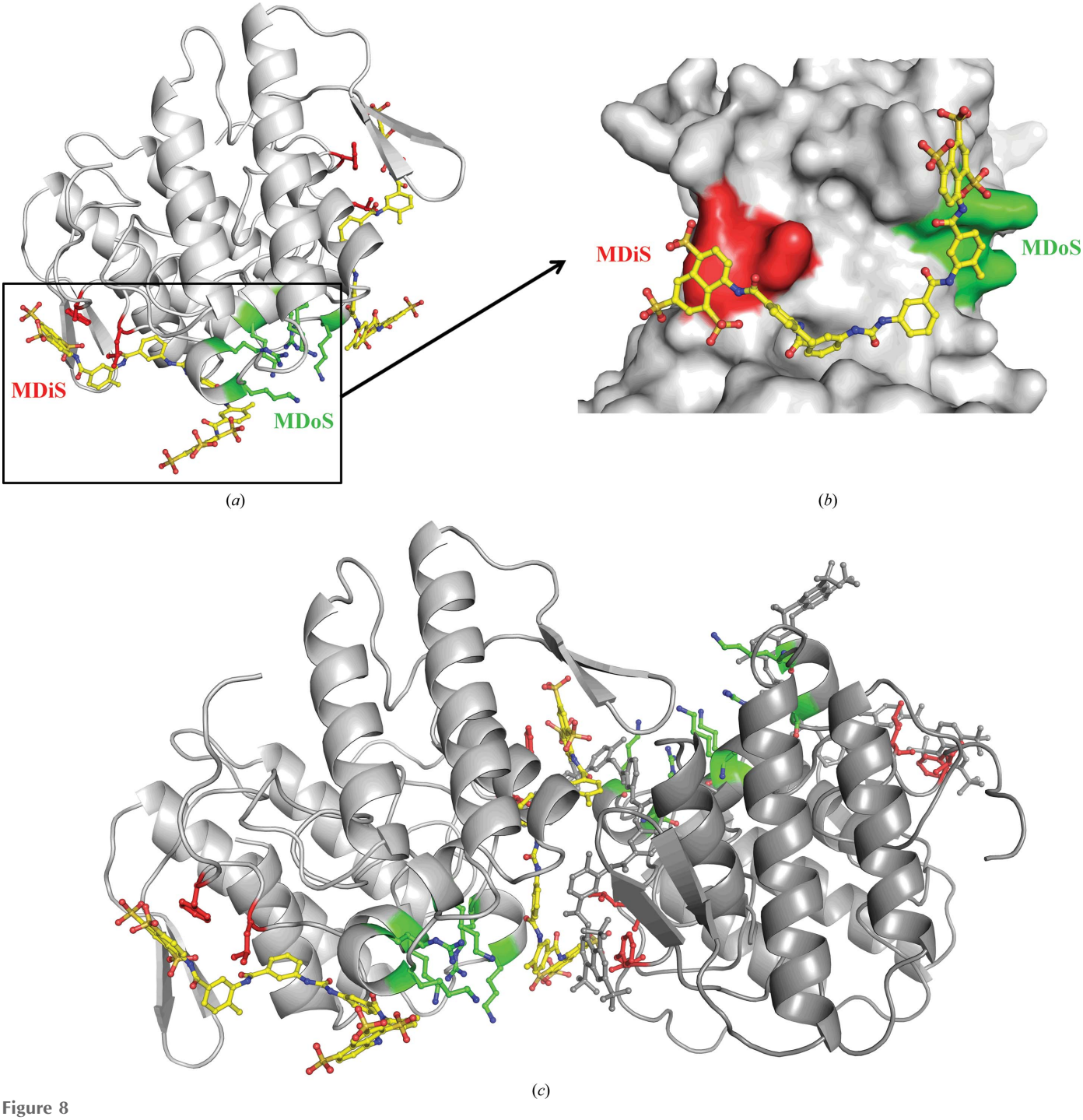


**Figure 8**
MDoS (cationic membrane-docking site) and MDiS (hydrophobic membrane-disruption site) in the MjTX-II–suramin structure, highlighting the interaction between the inhibitor and these sites. (*a*) Cartoon representation of the asymmetric unit of the crystal structure of the MjTX-II–suramin complex with the inhibitor interacting with MDoS (residues in green) and MDiS (residues in red). Suramin and the MDoS and MDiS residues are shown in ball-and-stick representation. (*b*) Detailed view of the interaction between a suramin molecule and a monomer of MjTX-II, highlighting the MDiS (red) and MDoS (green) regions. The protein is represented as a surface and the suramin ligand is shown in ball-and-stick representation. (*c*) Tetrameric conformation of the MjTX-II–suramin complex with the inhibitor interacting with the MDiS (red) and MDoS (green) regions.

MDoS burial process. Therefore, two synergic mechanisms can potentially explain the demonstrated inhibition of MjTX-II by suramin: (i) the suramin-binding mode on the toxin surface that results in a blockade of both the MDoS and MDiS sites, thus impairing toxin–membrane contacts (Figs. 8*a* and 8*b*), and (ii) MjTX-II–suramin-induced oligomerization resulting in a special protein–ligand quaternary arrangement that makes the MDoS and MDiS of all of the oligomerized toxins physically inaccessible (Fig. 8*c*).

### 4.4. Inhibitory mechanism of $PLA_2$-like toxins

As shown in §3.6, in the crystal structure of the BaspTX-II–suramin complex the suramin ligand interacts with the putative calcium-binding loop and C-terminal regions, obstructing the hydrophobic channel (Murakami *et al.*, 2005). By contrast, in the crystal structure of the ecarpholin S–suramin complex (Zhou *et al.*, 2008) interactions of the ligand with the C-terminal region were observed, particularly with Asn114, Lys115 and Lys116 (this basic cluster has been proposed to be part of the putative MDoS; Fernandes *et al.*, 2014). Similarly, suramin interacts with MjTX-II residues from the MDoS (Lys115 and Lys116) and MDiS (Leu122 and Phe126). Thus, despite the particularities of the interaction between suramin and MjTX-II or ecarpholin S, there are some similarities in the regions where the ligand binds to the toxins (MDoS region) and in the oligomerization process undergone by the toxins after ligand binding. These facts indicate that the inhibitory processes of suramin towards both proteins are related.

In addition to suramin, rosmarinic acid also showed efficient neutralizing characteristics for Lys49-$PLA_2$s (Ticli *et al.*, 2005; dos Santos, Cardoso *et al.*, 2011) and its complex has been crystallographically characterized (dos Santos, Cardoso *et al.*, 2011). The authors of this study observed that rosmarinic acid is bound at the entrance to the hydrophobic channel. Therefore, based on the proposed myotoxic mechanism, dos Santos, Cardoso *et al.* (2011) suggested that the inhibitory processes occur because of ligand steric hindrance that blocks the access of substrates to the hydrophobic channel.

Consequently, based on the effective inhibition by suramin and rosmarinic acid, we propose two modes of inhibition of $PLA_2$-like proteins: (i) ligands binding in the hydrophobic channel or blocking its access and (ii) ligands binding or blocking access to the MDoS and MDiS regions. The first inhibition mode avoids the binding of fatty acid to the toxin that is necessary to activate the protein *via* an oligomeric change, whereas the second mode avoids toxin docking and membrane disruption. Because suramin and rosmarinic acid act in both inhibitory processes, our experimental results are promising for their potential use as drugs against the local effects of myotoxic toxins.

## 5. Conclusions

In this study, we demonstrated that suramin is a potent inhibitor that binds to MjTX-II with high affinity. The crystal structure of the MjTX-II–suramin complex demonstrated for the first time an inhibitor that binds simultaneously to the sites of the toxin involved in membrane docking and disruption. Furthermore, the crystal structure, DLS and MD simulations identified the formation of higher-order oligomers (mainly tetramers), which also aids in the inhibitory process. The findings described in this work showed a great convergence with the data in the literature and with mechanism of action of $PLA_2$-like toxins proposed by our group in recent years. Based on these data, we suggest that suramin and other ligands (*e.g.* rosmarinic acid) should be clinically studied as inhibitors of the local myotoxic effects generated by $PLA_2$-like proteins.

## Acknowledgements

This work was financially supported by Fundação de Amparo à Pesquisa do Estado de São Paulo (FAPESP), Conselho Nacional de Desenvolvimento Científico e Tecnológico (CNPq) and Coordenação de Aperfeiçoamento de Pessoal de Nível Superior (CAPES), Brazil. We are grateful for the use of the Laboratório Nacional de Luz Síncrotron (LNLS), Brazil.

## References

Adams, P. D. *et al.* (2010). *Acta Cryst.* D**66**, 213–221.
Arni, R. K. & Ward, R. J. (1996). *Toxicon*, **34**, 827–841.
Arruda, E. Z., Silva, N. M., Moraes, R. A. & Melo, P. A. (2002). *Braz. J. Med. Biol. Res.* **35**, 723–726.
Azevedo, W. F. de, Ward, R. J., Lombardi, F. R., Giglio, J. R., Soares, A. M., Fontes, M. R. M. & Arni, R. K. (1997). *Protein Pept. Lett.* **4**, 329–334.
Burch, T. A. & Ashburn, L. L. (1951). *Am. J. Trop. Med. Hyg.* **31**, 617–623.
Cavalcante, W. L. G., Campos, T. O., Dal Pai-Silva, M., Pereira, P. S., Oliveira, C. Z., Soares, A. M. & Gallacci, M. (2007). *J. Ethnopharmacol.* **112**, 490–497.
Cavalcante, W. L. G., Silva, M. D. & Gallacci, M. (2005). *Chem. Biol. Interact.* **151**, 95–100.
Chen, V. B., Arendall, W. B., Headd, J. J., Keedy, D. A., Immormino, R. M., Kapral, G. J., Murray, L. W., Richardson, J. S. & Richardson, D. C. (2010). *Acta Cryst.* D**66**, 12–21.
Cherry, J. K. (1960). *East Afr. Med. J.* **37**, 550–558.
Chioato, L., De Oliveira, A. H. C., Ruller, R., Sá, J. M. & Ward, R. J. (2002). *Biochem. J.* **366**, 971–976.
Dennis, E. A., Cao, J., Hsu, Y.-H., Magrioti, V. & Kokotos, G. (2011). *Chem. Rev.* **111**, 6130–6185.
Ducruix, A. & Giegé, R. (1992). *Crystallization of Nucleic Acids and Proteins: A Pratical Approach.* Oxford University Press.
Emsley, P. & Cowtan, K. (2004). *Acta Cryst.* D**60**, 2126–2132.
Fathi, B., Harvey, A. L. & Rowan, E. G. (2011). *J. Venom Res.* **2**, 6–10.
Fernandes, C. A. H., Borges, R. J., Lomonte, B. & Fontes, M. R. M. (2014). *Biochim. Biophys. Acta*, **1844**, 2265–2276.
Fernandes, C. A. H., Comparetti, E. J., Borges, R. J., Huancahuire-Vega, S., Ponce-Soto, L. A., Marangoni, S., Soares, A. M. & Fontes, M. R. M. (2013). *Biochim. Biophys. Acta*, **1834**, 2772–2781.
Fernandes, C. A. H., Marchi-Salvador, D. P., Salvador, G. M., Silva, M. C. O., Costa, T. R., Soares, A. M. & Fontes, M. R. M. (2010). *J. Struct. Biol.* **171**, 31–43.
Freire, E., Schön, A. & Velazquez-Campoy, A. (2009). *Methods Enzymol.* **455**, 127–155.
Gallacci, M. & Cavalcante, W. L. G. (2010). *Toxicon*, **55**, 1–11.
Gallacci, M., Oliveira, M., Pai-Silva, M. D., Cavalcante, W. L. G. & Spencer, P. J. (2006). *Exp. Toxicol. Pathol.* **57**, 239–245.
Gunsteren, W. F. van & Berendsen, H. J. (1984). *J. Mol. Biol.* **176**, 559–564.
Gutiérrez, J. M. & Lomonte, B. (2013). *Toxicon*, **62**, 27–39.

Gutiérrez, J. M., Rucavado, A., Chaves, F., Díaz, C. & Escalante, T. (2009). *Toxicon*, **54**, 958–975.
Harvey, A. L., Barfaraz, A., Thomson, E., Faiz, A., Preston, S. & Harris, J. B. (1994). *Toxicon*, **32**, 257–265.
Heluany, N. F., Homsi-Brandeburgo, M. I., Giglio, J. R., Prado-Franceschi, J. & Rodrigues-Simioni, L. (1992). *Toxicon*, **30**, 1203–1210.
Henning, R. H., Rowan, E. G., Braga, M. F., Nelemans, A. & Harvey, A. L. (1996). *Eur. J. Pharmacol.* **301**, 91–97.
Hodgson, W. C. & Wickramaratna, J. C. (2002). *Clin. Exp. Pharmacol. Physiol.* **29**, 807–814.
Holland, D. R., Clancy, L. L., Muchmore, S. W., Ryde, T. J., Einspahr, H. M., Finzel, B. C., Heinrikson, R. L. & Watenpaugh, K. D. (1990). *J. Biol. Chem.* **265**, 17649–17656.
Krissinel, E. & Henrick, K. (2007). *J. Mol. Biol.* **372**, 774–797.
Lin, M.-J., Tan, C.-T., Lee, S.-Y. & Lin-Shiau, S.-Y. (2000). *Neurosci. Lett.* **287**, 97–100.
Lin-Shiau, S.-Y. & Lin, M.-J. (1999). *Eur. J. Pharmacol.* **382**, 75–80.
Lomonte, B., Angulo, Y. & Calderón, L. (2003). *Toxicon*, **42**, 885–901.
Lomonte, B., León, G., Angulo, Y., Rucavado, A. & Núñez, V. (2009). *Toxicon*, **54**, 1012–1028.
Lovell, S. C., Davis, I. W., Arendall, W. B., de Bakker, P. I. W., Word, J. M., Prisant, M. G., Richardson, J. S. & Richardson, J. S. (2003). *Proteins*, **50**, 437–450.
Magro, A. J., Fernandes, C. A. H., dos Santos, J. I. & Fontes, M. R. M. (2009). *Protein Pept. Lett.* **16**, 852–859.
Marcussi, S., Sant'Ana, C. D., Oliveira, C. Z., Rueda, A. Q., Menaldo, D. L., Beleboni, R. O., Stabeli, R. G., Giglio, J. R., Fontes, M. R. M. & Soares, A. M. (2007). *Curr. Top. Med. Chem.* **7**, 743–756.
McCoy, A. J. (2007). *Acta Cryst.* D**63**, 32–41.
Murakami, M. T., Arruda, E. Z., Melo, P. A., Martinez, A. B., Calil-Eliás, S., Tomaz, M. A., Lomonte, B., Gutiérrez, J. M. & Arni, R. K. (2005). *J. Mol. Biol.* **350**, 416–426.
Murakami, M. T., Viçoti, M. M., Abrego, J. R. B., Lourenzoni, M. R., Cintra, A. C. O., Arruda, E. Z., Tomaz, M. A., Melo, P. A. & Arni, R. K. (2007). *Toxicon*, **49**, 378–387.
Oliveira, M. de, Cavalcante, W. L. G., Arruda, E. Z., Melo, P. A., Dal-Pai Silva, M. & Gallacci, M. (2003). *Toxicon*, **42**, 373–379.
Oliveira, R. C. W. de (2009). *Animais Peçonhentos do Brasil: Biologia, Clínica e Terapêutica dos Envenenamentos*, p. 550. São Paulo: Sarvier.
Oostenbrink, C., Soares, T. A., van der Vegt, N. F. & van Gunsteren, W. F. (2005). *Eur. Biophys. J.* **34**, 273–284.
Oshima-Franco, Y., Leite, G. B., Belo, C. A. D., Hyslop, S., Prado-Franceschi, J., Cintra, A. C. O., Giglio, J. R., da Cruz-Hofling, M. A. & Rodrigues-Simioni, L. (2004). *Pharmacol. Toxicol.* **95**, 175–182.
Otero, R. *et al.* (2002). *Toxicon*, **40**, 1107–1114.
Otwinowski, Z. & Minor, W. (1997). *Methods Enzymol.* **276**, 307–326.
Ownby, C. L., Selistre de Araujo, H. S., White, S. P. & Fletcher, J. E. (1999). *Toxicon*, **37**, 411–445.
Ponce-Soto, L. A., Barros, J. C., Marangoni, S., Hernandez, S., Dal Belo, C. A., Corrado, A. P., Hyslop, S. & Rodrigues-Simioni, L. (2009). *Comp. Biochem. Physiol. C Toxicol. Pharmacol.* **150**, 291–297.
Randazzo-Moura, P., Ponce-Soto, L. A., Rodrigues-Simioni, L. & Marangoni, S. (2008). *Protein J.* **27**, 355–362.
Rodrigues, V. M., Marcussi, S., Cambraia, R. S., de Araújo, A. L., Malta-Neto, N. R., Hamaguchi, A., Ferro, E. A., Homsi-Brandeburgo, M. I., Giglio, J. R. & Soares, A. M. (2004). *Toxicon*, **44**, 305–314.
Salvador, G. H. M., Cavalcante, W. L. G., dos Santos, J. I., Gallacci, M., Soares, A. M. & Fontes, M. R. M. (2013). *Toxicon*, **72**, 52–63.
Salvador, G. H. M., Fernandes, C. A. H., Magro, A. J., Marchi-Salvador, D. P., Cavalcante, W. L. G., Fernandez, R. M., Gallacci, M., Soares, A. M., Oliveira, C. L. P. & Fontes, M. R. M. (2013). *PLoS One*, **8**, e60610.
Santos, J. I. dos, Cardoso, F. F., Soares, A. M., dal Pai Silva, M., Gallacci, M. & Fontes, M. R. M. (2011). *PLoS One*, **6**, e28521.
Santos, J. I. dos, Cintra-Francischinelli, M., Borges, R. J., Fernandes, C. A. H., Pizzo, P., Cintra, A. C. O., Braz, A. S. K., Soares, A. M. & Fontes, M. R. M. (2011). *Proteins* **79**, 61–78.
Santos, J. I. dos, Soares, A. M. & Fontes, M. R. M. (2009). *J. Struct. Biol.* **167**, 106–116.
Schneider, J. (1963). *Bull. World Health Organ.* **28**, 763–786.
Scott, D. L. & Sigler, P. B. (1994). *Adv. Protein Chem.* **45**, 53–88.
Soares, A. M., Andrião-Escarso, S. H., Bortoleto, R. K., Rodrigues-Simioni, L., Arni, R. K., Ward, R. J., Gutiérrez, J. M. & Giglio, J. R. (2001). *Arch. Biochem. Biophys.* **387**, 188–196.
Soares, A. M., Rodrigues, V. M., Homsi-Brandeburgo, M. I., Toyama, M. H., Lombardi, F. R., Arni, R. K. & Giglio, J. R. (1998). *Toxicon*, **36**, 503–514.
Stábeli, R. G., Amui, S. F., Sant'Ana, C. D., Pires, M. G., Nomizo, A., Monteiro, M. C., Romão, P. R. T., Guerra-Sá, R., Vieira, C. A., Giglio, J. R., Fontes, M. R. & Soares, A. M. (2006). *Comp. Biochem. Physiol. C Toxicol. Pharmacol.* **142**, 371–381.
Ticli, F. K., Hage, L. I. S., Cambraia, R. S., Pereira, P. S., Magro, A. J., Fontes, M. R. M., Stábeli, R. G., Giglio, J. R., França, S. C., Soares, A. M. & Sampaio, S. V. (2005). *Toxicon*, **46**, 318–327.
Van Der Spoel, D., Lindahl, E., Hess, B., Groenhof, G., Mark, A. E. & Berendsen, H. J. (2005). *J. Comput. Chem.* **26**, 1701–1718.
Vega, S., Abian, O. & Velazquez-Campoy, A. (2015). *Methods*, **76**, 99–115.
Wallace, A. C., Laskowski, R. A. & Thornton, J. M. (1995). *Protein Eng. Des. Sel.* **8**, 127–134.
Ward, R. J., Chioato, L., de Oliveira, A. H. C., Ruller, R. & Sá, J. M. (2002). *Biochem. J.* **362**, 89–96.
Watanabe, L., Soares, A. M., Ward, R. J., Fontes, M. R. M. & Arni, R. K. (2005). *Biochimie*, **87**, 161–167.
Wiederstein, M. & Sippl, M. J. (2007). *Nucleic Acids Res.* **35**, W407–W410.
Williams, D., Gutiérrez, J. M., Harrison, R., Warrell, D. A., White, J., Winkel, K. D. & Gopalakrishnakone, P. (2010). *Lancet*, **375**, 89–91.
Williamson, J. & Desowitz, R. S. (1956). *Nature (London)*, **177**, 1074–1075.
Zhou, X., Tan, T.-C., Valiyaveettil, S., Go, M. L., Manjunatha Kini, R., Velazquez-Campoy, A. & Sivaraman, J. (2008). *Biophys. J.* **95**, 3366–3380.